



HAL
open science

Effect of local stress heterogeneities on dislocation fields: Examples from transient creep in polycrystalline ice

S. Piazzolo, M. Montagnat, F. Grennerat, H. Moulinec, J. Wheeler

► To cite this version:

S. Piazzolo, M. Montagnat, F. Grennerat, H. Moulinec, J. Wheeler. Effect of local stress heterogeneities on dislocation fields: Examples from transient creep in polycrystalline ice. *Acta Materialia*, 2015, 90, pp.303-309. 10.1016/j.actamat.2015.02.046 . hal-01746106

HAL Id: hal-01746106

<https://hal.science/hal-01746106>

Submitted on 29 Mar 2018

HAL is a multi-disciplinary open access archive for the deposit and dissemination of scientific research documents, whether they are published or not. The documents may come from teaching and research institutions in France or abroad, or from public or private research centers.

L'archive ouverte pluridisciplinaire **HAL**, est destinée au dépôt et à la diffusion de documents scientifiques de niveau recherche, publiés ou non, émanant des établissements d'enseignement et de recherche français ou étrangers, des laboratoires publics ou privés.

Effect of local stress heterogeneities on dislocation fields: Examples from transient creep in polycrystalline ice.

S. Piazzolo^a, M. Montagnat^{b,c}, F. Grennerat^{b,c}, H. Moulinec^d, J. Wheeler^e

^aARC Center of Excellence for Core to Crust Fluid Systems (CCFS) and GEMOC, Department of Earth and Planetary Science, Macquarie University, NSW 2109, Australia

^bCNRS, LGGE, UMR5183, 54 rue Molière, 38041 Grenoble, France

^cUniv. Grenoble Alpes, LGGE, 38041 Grenoble, France

^dLaboratoire de Mécanique et d'Acoustique, CNRS, UPR7051, Aix Marseille University, Centrale Marseille, 31 Chemin Joseph Aiguier, 13402 Marseille Cedex 20, France

^eDepartment of Earth and Ocean Sciences, School of Environmental Science, Liverpool University, Liverpool L69 3GP, UK

Abstract

This work presents a coupled experimental and modeling approach to better understand the role of stress field heterogeneities on deformation behavior in material with a high viscoplastic anisotropy e.g. polycrystalline ice. Full-field elasto-viscoplastic modeling is used to predict the local stress and strain field during transient creep in a polycrystalline ice sample. Modeling input includes the experimental starting microstructure and a validated slip system dependent flow law. EBSD measurements on selected areas are used to estimate the local dislocation field utilizing the Weighted Burgers Vector (WBV) analysis. Areas of local stress concentration correlate with triple junctions and grain boundaries, originating from strain incompatibilities between differently oriented grains. In these areas of highly heterogeneous stress patterns, (a) kink bands are formed and (b) WBV analysis shows a non-negligible c-axis component of the WBV. The correlation between this defect structure and presence of kink bands suggest that kink band formation is an efficient accommodation deformation mode.

This is the author version of the paper, find the editor one at <http://dx.doi.org/10.1016/j.actamat.2015.02.046>

Keywords:

stress heterogeneities, dislocation field, electron backscatter diffraction, full-field modeling, kink bands, viscoplastic anisotropy

1. Introduction

When polycrystalline material is plastically deforming, stress and strain heterogeneity fields are developing due to strain incompatibilities between grains of different crystallographic orientations. Depending on the level of viscoplastic anisotropy of the material, the heterogeneity amplitude can be high.

The viscoplastic anisotropy of ice is known to be very strong, with dislocations gliding mostly on the basal plane with three equivalent $\langle 11\bar{2}0 \rangle$ Burgers vector directions [1]. This results in strong kinematic hardening at grain boundaries and triple junctions [2]. As such ice is a good model for materials with high viscoplastic anisotropy, such as magnesium [3, 4], quartz [5] and olivine [6]. In ice, strong heterogeneity fields were measured by Digital Image Correlation on polycrystalline samples deformed by compression

creep with local strain amplitude as high as ten times the macroscopic strain [7]. The strain heterogeneities were also indirectly observed through lattice misorientation measurements via EBSD [8, 9] and were simulated using full-field viscoplastic approaches based on Fast Fourier Transform formulation [10, 9, 7]. In these modelling approaches, plasticity is simulated by the activation of several slip systems (e.g. basal, prismatic and pyramidal slip in the case of ice), where each slip system is assigned a relative critical resolved shear stress for slip activation. In this frame, these last works have shown, among other results, that observed high stress and strain heterogeneities could only be correctly simulated providing a significant amount of non-basal slip activity in the corresponding areas, while the global non-basal activity remained low [10, 9]. The same numerical constraint was derived for polycrystalline Mg in conditions where twinning was

not activated [11]. However, up to now there exists no unequivocal evidence for macroscopic strain resulting from non-basal slip in ice [12, 13].

The presence of heterogeneous dislocation fields in experimentally and naturally deformed ice was mostly observed indirectly from substructures observations (X-ray diffraction, optical analyses, EBSD...) [8, 9, 14, 15]. In particular kink bands and double kink bands has been commonly observed in polycrystalline ice deformed in the laboratory. The origin of these kink bands was indirectly interpreted to be related to some non-basal dislocation activity like climb or cross-slip [8, 9].

The objective of the present work is to couple both modeling and high resolution EBSD observations in order to extract a more direct causal relationship between stress and dislocation fields. These relationships are expected to be of particular significance in polycrystalline materials composed of phases exhibiting a strong viscoplastic anisotropy.

2. Experiment and EBSD analyses

Both modeling and experimental analyses were performed on the basis of compression creep experiments on samples made of laboratory grown polycrystalline ice with columnar grain shape [9]. Tests were stopped at 1% strain in order to prevent the initiation of recrystallization processes. A constant 0.5 MPa stress was applied at -10°C , with columns perpendicular to the compression direction (see [7] for details). Grain size of the order of 1 μm enabled high resolution observations in terms of microstructure and crystal orientation variations at grain boundaries, triple junctions and grain interiors. The deformed microstructure is shown in Fig. 1. In all analyses the same XYZ sample coordinate system is used where Z is out of plane and the Y direction is parallel to the main compression axis.

EBSD analysis was performed on a Philips XL-30-ESEM-FEG at the Department of Geological Sciences at Stockholm University. EBSD patterns were auto-indexed using the CHANNEL 5 software of OI-HKL Technology. Samples analysed were extracted from the deformed sample. They were uncoated, kept at high vacuum and frozen to the pre-tilted sample holder sledge cooled to temperature of -90 to -100°C using a cold stage (for more details see [8]). Data were collected by moving the beam across a rectangular area at steps of $15\ \mu\text{m}$. Noise reduction was performed following [16, 17]. Accuracy of EBSD data is within 0.3° - 0.4° [18]. Fig. 1 presents selected EBSD maps

showing the local variations in orientations.

3. Weighted Burgers Vector analysis

To quantitatively analyze the EBSD point grid data we utilized the Weighted Burgers Vector (WBV) analysis explained in details in [19]. The WBV is a recently developed new quantity to constrain dislocation densities and dislocation types using EBSD data on two dimensional sections through crystalline materials. The WBV is defined as the sum, over all dislocation types, of [(density of intersections of dislocation lines with a map) \times (Burgers vector)] and as such can be calculated from a planar set of orientation measurements such as in an EBSD orientation map. There is no assumption about the orientation gradient in the third dimension. The magnitude of the WBV gives a lower bound of the magnitude of the dislocation density tensor. The direction of the WBV can be used to constrain the types of Burgers vectors of the geometrically necessary dislocations present in the microstructure and their geometric relationship to intra-grain structures, for example subgrain walls. The WBV can then be decomposed in terms of the 3 main lattice vectors [20]. In the case of ice, the two a-axis lattice vectors are further decomposed into the 3 equivalent a-axis lattice vectors. We can calculate the net Burgers vector content of dislocations intersecting a given area of a map by an integration around the edge of this area. This integral WBV method is fast, complements point-by-point WBV calculations and, thanks to this integration, reduces the effect of noise on the analysis. A lower bound of the density of geometrically necessary dislocations can be estimated from this calculation. This estimation is not absolute but can be used for comparison purposes. It should be noted that the net Burgers vector value derived using the integral WBV method is sensitive to the chosen area both in terms of size and location.

WBV analysis data is represented in color coded maps showing the WBV magnitude, WBV directions as projected arrows onto the color coded maps and in pole figures with both the sample coordinate system and the crystal coordinate system (see Fig. 2).

Table 1 presents the integral WBV calculated over selected areas in the analyzed samples (Fig. 2 and Fig. 3), decomposed into the three a-axes and the c-axis of the ice crystallographic structure. Areas were selected to represent the observed spectrum of different microstructures present within the analyzed sample. Such microstructures include triple junctions, grain boundaries with or without asperities, areas in close vicinity or at

135 distance to grain boundaries. Data from Table 1 shows 185
136 that the integral WBV values vary significantly depend- 186
137 ing on microstructure type and location. However, for 187
138 each selected area, we obtained several WBV values 188
139 and chose to present here values that are representative 189
140 for the selected area. 190

141 The accuracy of the integral WBV is dependent on the 191
142 angular resolution of the EBSD data. Using EBSD 192
143 data with high angular resolution (here within 0.3 de- 193
144 grees), we consider an integral WBV ratio of one spec- 194
145 ific Burger vector over the maximum WBV value of 195
146 0.5 **significant**. 196

147 4. Local stress field estimation

148 Full-field numerical simulations were performed 200
149 using the CraFT code as presented in [21]. The code is 201
150 based on the FFT method initially proposed in [22, 23], 202
151 extended to elasto-viscoplastic composites using a 203
152 step-by-step integration in time in [24] (see also the 204
153 numerical details in [21]). The method used in the 205
154 CraFT code finds a strain rate field associated with a 206
155 kinematically admissible velocity field that minimizes 207
156 the average local work rate under the compatibility and 208
157 equilibrium constraints. An iterative scheme is used 209
158 following a fixed point approach. It is numerically 210
159 more efficient than the finite element method [25], 211
160 but is limited to simulations with microstructures with 212
161 periodic boundary conditions.

162 The specimen undeformed microstructure was dis- 213
163 cretized into 512×512 Fourier points with a single 214
164 layer of Fourier points in the third (Z) direction, 215
165 assuming thus infinite column length. To represent the 216
166 microstructure, each Fourier point is allocated a c-axis 217
167 orientation according to the measured orientation of 218
168 the underformed experimental sample. Consequently 219
169 grain boundary are not specifically defined as discrete 220
170 objects with specific physical characteristics other than 221
171 a change in crystal orientation. Throughout the numeri- 222
172 cal simulations, no crystallographic orientation changes 223
173 are imposed, thus the microstructure (orientation, grain 224
174 boundaries) does not evolve.

175 Creep conditions equivalent to the experimental ones 225
176 were applied (constant 0.5 MPa stress in the vertical 226
177 direction, transient creep up to 1% macroscopic strain). 227
178 The exact experimental boundary conditions (stress free 228
179 lateral surface) could not be reproduced due to the nu- 229
180 merical periodicity constraint. therefore, Accordingly, 230
181 stress and strain fields predicted close to the specimen 231
182 edges are not expected to be very accurate, however 232
183 Grennerat et al. [7] showed a limited impact on the 233
184 macroscopic response and estimated fields, especially

in the center of the modeled microstructure, where the 185
186 areas of interest here are located.

The elasto-viscoplastic response of ice was modeled 187
188 following the law and hypothesis discussed in details in 189
190 [21]. To model ice, the used crystal plasticity formula- 191
192 tion accounts for three different families of slip systems, 193
194 namely the basal, prismatic and pyramidal systems, 195
196 the latter two being taken stiffer than basal slip. A 197
198 power law is considered for the evolution of the shear 199
200 strain rate as a function of the resolved shear stress on 201
202 each slip system that integrates kinematic hardening, 203
204 slip system interactions and their evolution with time 205
206 during transient creep. The material parameters of the 207
208 law were determined by adjusting them according to 209
210 experimental data available for single crystals as well 211
212 as for polycrystals, as detailed in [21]. The Critical 213
214 Resolved Shear Stress (CRSS) on each slip system 215
216 was allowed to evolve with strain between initial and 217
218 stationary values. Table 2 provides the relative CRSS 219
220 for each slip system family, and the value of the stress 221
222 exponent attributed to each family. It is worth noting 223
224 that the relative CRSS is much higher for the pyramidal 225
226 family, and that there is a relative softening of basal 227
228 systems during transient creep [21].

The local heterogeneities of the strain and stress fields 229
230 are illustrated in Fig. 4a) and b) where the spatial 231
232 variation of the equivalent stress ($\sigma_{eq} = \sqrt{\frac{3}{2}\sigma_{ij}\sigma_{ij}}$) 233
234 and equivalent strain ($\varepsilon_{eq} = \sqrt{\frac{3}{2}\varepsilon_{ij}\varepsilon_{ij}}$) are repre- 235
236 sented, respectively. For each simulated pixel of 237
238 the microstructure, the deviatoric part of the stress 239
240 tensor was decomposed into its eigenvector frame. 241
242 From this decomposition, we extracted the eigenvector 243
244 corresponding to the largest absolute eigenvalue. We 245
246 built a composite vector representation based on the 247
248 in-plane projection of a vector having the direction of 249
250 this eigenvector, and the amplitude of the associated 251
252 eigenvalue. This representation is given in Fig. 4c) for 253
254 the area of interest, superimposed on the equivalent 255
256 stress contour plot.

255 5. Discussion

Numerical modeling shows that local stress concen- 256
257 trations and stress field heterogeneities occur close to 258
259 triple junctions and grain boundaries. The higher the 260
261 mismatch between crystallographic grain orientations, 262
263 the higher the concentration and heterogeneities (Fig. 264
265 4). For example, the triple junctions between grains 266
267 that are similarly oriented show less stress and strain 268

233 heterogeneities (between grains 1, 4 and 5) than that 285
 234 between differently oriented grains (grains 1, 2 and 3). 286
 235 In addition, the relative orientation of grain boundary to 287
 236 grain orientation influences the stress distribution. For 288
 237 example, at the boundary between grains 1 and grain 4 289
 238 we observe a zone of high stress (Fig. 4c) where there 290
 239 is a change in the grain boundary orientation relative to 291
 240 the grain orientations. 292
 241 Similarly, WBV analyses show that commonly WBV 293
 242 magnitude associated with subgrain wall is highest 294
 243 close to the grain boundary and decreases towards the 295
 244 grain centre (Fig. 2). 296
 245 Although the resolution of the model microstructure 297
 246 is not as high as the one measured, there exists a 298
 247 close correlation between the characteristics of the 299
 248 stress heterogeneities (amplitude and direction of stress 300
 249 field), and the amplitude and location of the lattice 301
 250 misorientations measured by EBSD (see Fig. 3). This 302
 251 is pronounced in areas close to triple junction, but also 303
 252 apparent within the grain interior as shown in map G1, 304
 253 Fig. 3 where the heterogenous stress band crossing 305
 254 grain 1 correlates well with the observed subgrain 306
 255 boundary crossing the corresponding EBSD map. In 307
 256 general, areas which show high stress in simulation 308
 257 are also characterized by high net Burger vector values 309
 258 (e.g. MapG1 areaA, MapG4-1-5 areaE). 310
 259 Areas close to triple junctions present WBV dominated 311
 260 by one a-axis direction or a combination of two a-axes. 312
 261 This is illustrated by the decomposition of the integral 313
 262 WBV data (Table 1) and represented in the inverse pole 314
 263 figure plots in Fig. 3 (see for instance mapG1-3 areas A 315
 264 and B and mapG4-1-5 area B, Table 1). 316
 265 As illustrated by the inverse pole figure of subarea D 317
 266 from map G4-1-5, there is a systematic presence of a 318
 267 minor but significant c-axis component close to triple 319
 268 junctions. Such a c-axis component is considered as 320
 269 non-negligible when the ratio $K_c/\max(K_{ai})$ is higher 321
 270 than 0.5 (see Table 1). In contrast, most of the areas 322
 271 analyzed in a grain interior show a c-axis component of 323
 272 the WBV which is very close to the detection limit (see 324
 273 Table 1). 325
 274 Close to triple junctions, we observe near straight 326
 275 subgrain boundaries. Their traces are parallel to the 327
 276 c-axis, and the WBV are predominantly oriented along 328
 277 the a-axis perpendicular to the subgrain boundary trace 329
 278 (Fig. 1 and Fig. 3). The other a-axis contribution is 330
 279 related to a continuous crystal bending perpendicular to 331
 280 the c-axis (see Fig. 5 with a sketch of the bending axis). 332
 281 Similar observations were made in [8, 9]. 333
 282 These only slightly curved subgrain boundaries com- 334
 283 monly occur in parallel pairs with the main WBV 335
 284 pointing in opposite directions (Fig. 3 mapG1-3 336

and mapG4-1-5, Table 1). The parallelism of the
 subgrain boundary traces, their orientation relative to
 the crystallographic axes of the host grain together
 with the orientation of the main WBV a-axis compo-
 nent is consistent with a strongly crystallographically
 determined boundary development. The opposing
 directions of WBV in pairs of subgrain boundaries
 (Fig. 3) is consistent with kink bands with alternating
 opposing dislocation structures [26, 27, 28]. These
 crystallographically well defined kink boundaries could
 appear similar to the twinning modes in magnesium
 in the way that they both accommodate shear stress
 that cannot be resolved by the easy slip system i.e.
 basal slip in ice [3, 4, 29]. In metals, kink bands
 can occur at large deformation as strain localization
 modes, as predicted by the bifurcation analysis of
 [30], but also at the early stage of deformation in the
 presence of obstacles [31]. Chang et al. [31] used
 Dislocation Dynamic simulation to illustrate the stable
 position of an edge dislocation within the stress field
 of an alignment of edge dislocations forming the kink
 band. Consequently, in contrast to what was initially
 thought [9], climb or cross-slip do not seem to be
 necessary mechanisms to explain kink band formation.
 In summary, observations suggest that kink bands form
 in areas of very high local stress fields originating
 either from strain incompatibilities developed in materials
 with high viscoplastic anisotropies or from high strain
 rates.

It should be noted that the used numerical model does
 not account for specific grain boundary properties. The
 question of the strain continuity at an interface such as
 grain boundary is therefore not addressed. In contrast,
 recent work [32] showed that stress accumulation at
 boundaries can explain grain boundary delamination
 in alloys. In the case of ice deforming during tran-
 sient creep under low applied stress, no cracking was
 observed at grain boundaries, but a better account for
 continuity conditions of the plastic distortion at GB
 might be necessary to evaluate the impact of strain
 heterogeneities on recrystallization mechanisms for
 instance.

Our data show that in high stress concentration areas,
 close to triple junctions, a Burgers vector component
 parallel to c-axis is present. Cross slip of dislocations
 with Burgers vector lying in the basal plane cannot
 explain this; instead it could be interpreted by a local
 activity of a non-basal slip system. Conceptually,
 such a non-basal slip activity is expected only in such
 high stress areas, as non-basal activity requires high
 level of local stress in order to overcome the high
 critical resolved shear stress required for non-basal slip

[1]. So far, the very few observations on non-basal dislocation activity in ice were performed in conditions with very few dislocations activated, that could hardly be extrapolated. Indeed, they were performed using X-ray diffraction topography which enable individual dislocation observation at the very early stage of deformation [33, 34].

The observed crystal bending parallel as well as perpendicular to the kink bands which is accommodated by the shown presence of Burgers vectors along not one but two a-axes in high stress areas, may results in the development of subgrain boundaries both parallel and perpendicular to c-axis. This then will result in the formation of a subgrain with near perpendicular subgrain boundaries, one parallel to c-axis and one perpendicular to c-axis. Such a developing subgrain is shown in Fig. 5 and has been described in [8]. This subgrain boundary formation represents one of the recrystallization processes relaxing strain heterogeneities at macroscopic strain exceeding the transient creep regime [2, 35].

In summary:

- Coupled full field elasto-viscoplastic modelling and detailed EBSD analysis show the effect of stress heterogeneities (magnitude and orientation) on the dislocation field.
- The WBV c-axis component measured in high stress areas could be consistent with local activation of non-basal slip.
- At low strain, formation of kink bands with a well defined crystallographic character appears as an efficient accommodation deformation mode, similar to twinning in Mg.
- Distinct misorientations across and perpendicular to kink boundaries form substructures which act as precursors for grain nucleation.
- The approach presented is applicable to materials with significant viscoplastic anisotropy.

Acknowledgments: Financial support by French ANR is acknowledged (project ELVIS, #ANR-08-BLAN-0138, project DREAM #ANR-13-BS09-0001). Together with support from institutes INSIS and INSU of CNRS, France. The authors gratefully acknowledge the ESF Research Networking Programme Micro-Dynamics of Ice (www.microdice.eu). MM is part of Labex OSUG@2020 (ANR10 LABX56). SP acknowledges the financial support of the European Science

Foundation under the EUROCORES Programme, EuroMinSci, MinSubStrDyn, No. ERAS-CT-2003-980409 of the European Commission, DG Research, FP6. SP acknowledges additional funding from ARC DP120102060 and FT1101100070. Funding by ARC Centre of Excellence for Core to Crust Fluid Systems (www.CCFS.mq.edu.au) allowed a Research visit of M.M. to Macquarie University. This is contribution 534 from the ARC Centre of Excellence for Core to Crust Fluid Systems (<http://www.ccfs.mq.edu.au>) and 975 in the GEMOC Key Centre. Funding from the Australian Research Council (ARC) through the CCFS Visiting Researcher scheme is gratefully acknowledged (www.GEMOC.mq.edu.au).

- [1] Hondoh T. In: T Hondoh (Ed.), Physics of Ice Core Records. Sapporo: Hokkaido University Press, 2000, 2–34.
- [2] Duval P, Ashby M, Anderman I. J Phys Chem 1983;87:4066.
- [3] Barnett MR. Materials Science and Engineering: A 2007;464:1.
- [4] Barnett MR. Materials Science and Engineering: A 2007;464:8.
- [5] Hobbs BE. Preferred orientation in deformed metals and rocks, chapter The geological significance of microfabric analyses. Academic Press, Orlando, 1985, 463–484.
- [6] Nicolas A, Poirier JP. Crystalline Plasticity and Solid State Flow in Metamorphic Rocks. John Wiley & Sons, 1976.
- [7] Grennerat F, Montagnat M, Castelnau O, Vacher P, Moulinec H, Suquet P, Duval P. Acta Materialia 2012;60:3655.
- [8] Piazzolo S, Montagnat M, Blackford JR. Journal of Microscopy 2008;230:509.
- [9] Montagnat M, Blackford JR, Piazzolo S, Arnaud L, Lebensohn RA. Earth and Planetary Science Letters 2011;305:153 .
- [10] Lebensohn RA, Montagnat M, Mansuy P, Duval P, Meyssonier J, Philip A. Acta Materialia 2009;57:1405 .
- [11] Martin G, Sinclair CW, Lebensohn RA. Materials Science and Engineering: A 2014;603:37.
- [12] Shearwood C, Whitworth RW. Phil Mag 1991;A64:289.
- [13] Louchet F. C R Physique 2004;5:687.
- [14] Montagnat M, Duval P, Bastie P, Hamelin B, Lipenkov VY. Earth and Planetary Science Letters 2003;214:369 .
- [15] Donges J, Montagnat M, Bastie P, Grennerat F. Nuclear Instruments and Methods in Physics Research Section B: Beam Interactions with Materials and Atoms 2013;300:6 .
- [16] Prior D. Journal of Microscopy 1999;195:217.
- [17] Piazzolo S, Bestmann M, Prior DJ, Spiers CJ. Tectonophysics 2006;427:55.
- [18] Borthwick VE, Piazzolo S. Journal of Structural Geology 2010; 32:982.
- [19] Wheeler J, Mariani E, Piazzolo S, Prior DJ, Trimby P, Drury MR. Journal of Microscopy 2009;233:482.
- [20] Wenk RH, Bulakh A. Minerals: Their Constitution and Origin. Cambridge Univ. Press, 2004.
- [21] Suquet P, Moulinec H, Castelnau O, Montagnat M, Lahellec N, Grennerat F, Duval P, Brenner R. Procedia IUTAM 2012;3:76.
- [22] Moulinec H, Suquet P. Computer Methods in Applied Mechanics and Engineering 1998;157:69 .
- [23] Moulinec H, Suquet P. European Journal of Mechanics - A/Solids 2003;22:751.
- [24] Idiart MI, Moulinec H, Ponte Castañeda P, Suquet P. Journal of the Mechanics and Physics of Solids 2006;54:1029 .
- [25] Prakash A, Lebensohn RA. Modelling Simul Mater Sci Eng 2009;17:1.

- 446 [26] Wilson C, Burg J, Mitchell J. *Tectonophysics* 1986;127:27.
447 [27] Nishikawa O, Takeshita T. *Tectonophysics* 1999;301:21 .
448 [28] Yamasaki M, Hagihara K, ichi Inoue S, Hadorn JP, Kawamura
449 Y. *Acta Materialia* 2013;61:2065 .
450 [29] Chapuis A. *Materials Science and Engineering: A* 2014;
451 590:401.
452 [30] Sedláček R, Blum W, Kratochvíl J, Forest S. *Metallurgical and*
453 *Materials Transactions A* 2002;33:319.
454 [31] Chang HJ, Gaubert A, Fivel M, Berbenni S, Bouaziz O, Forest
455 S. *Computational Materials Science* 2012;52:33.
456 [32] Messner MC, Beaudoin AJ, Dodds Jr RH. *Engineering Fracture*
457 *Mechanics* 2015;133:70.
458 [33] Shearwood C, Withworth R. *JGlaciol* 1989;35:281.
459 [34] Shearwood C, Whitworth R. *Acta Metall Mater* 1993;41:205.
460 [35] Montagnat M, Durand G, Duval P. *Supp Issue Low Temperature*
461 *Science* 2009;68:81.

Analyses areas		Integral WBV (μm^{-2})					ρ
Map	gr/area	K_{a1}	K_{a2}	K_{a3}	K_c	$K_c/\max(K_{ai})$	(10^{10}m^{-2})
MapG2	2/A	-0.32	0.28	0.04	0.05	0.156	18.49
	2/B	0.18	-0.15	-0.03	0.02	0.111	5.62
MapG1	1/A	0.08	-0.01	-0.07	-0.02	0.250	1.18
	1/B*	-0.01	0.01	0.01	0.01		0.04
MapG1-3	1/A	-0.28	0.11	0.18	0.08	0.282	12.93
	1/B	0.73	-0.43	-0.30	-0.12	0.164	82.22
	3/C	0.29	-0.13	-0.15	-0.1	0.349	13.35
MapG4-1-5	1/A	-0.19	0.05	0.13	0.11	0.589	6.76
	1/B	0.10	-0.03	-0.06	0.04	0.414	1.61
	4/C	0.09	-0.06	-0.02	-0.01	0.115	1.22
	4/D	0.05	-0.01	-0.05	-0.20	3.750	4.51
	5/E	0.44	-0.30	-0.13	-0.29	0.664	38.46

Table 1: Integral WBV decomposed onto the three crystallographic axis of the ice crystal, for specific areas in EBSD maps shown in Figs. 1, 2 and 3. The two K_a vector directions are symmetrically equivalent, they were decomposed into the 3 a-directions following [20]. The relative activity of $K_c/\max(K_{ai})$ is also given. ρ provides a lower bound estimate of the geometrically necessary dislocation density in the area. Step size is $15\mu\text{m}$ for all EBSD maps. * minimum value of the net Burgers vector magnitude. "gr" signifies grain number (cf. Fig. 1) and "area", subarea as shown in Figs. 2 and 3.

System family	τ_{iniR}	τ_{statR}	n_s
basal	1	1	2
prismatic	1.3	68.2	2.85
pyramidal	38.75	176	4

Table 2: Relative CRSS for the three slip system families at the beginning of the transient creep, τ_{iniR} , and at the end, τ_{statR} . n_s is the stress exponent that was adjusted by [21] for each family. The absolute value of τ_{mi} for the basal slip systems was fitted at 0.1 by [21], and the absolute value of τ_{stat} for the basal slip systems was fitted at 0.022.

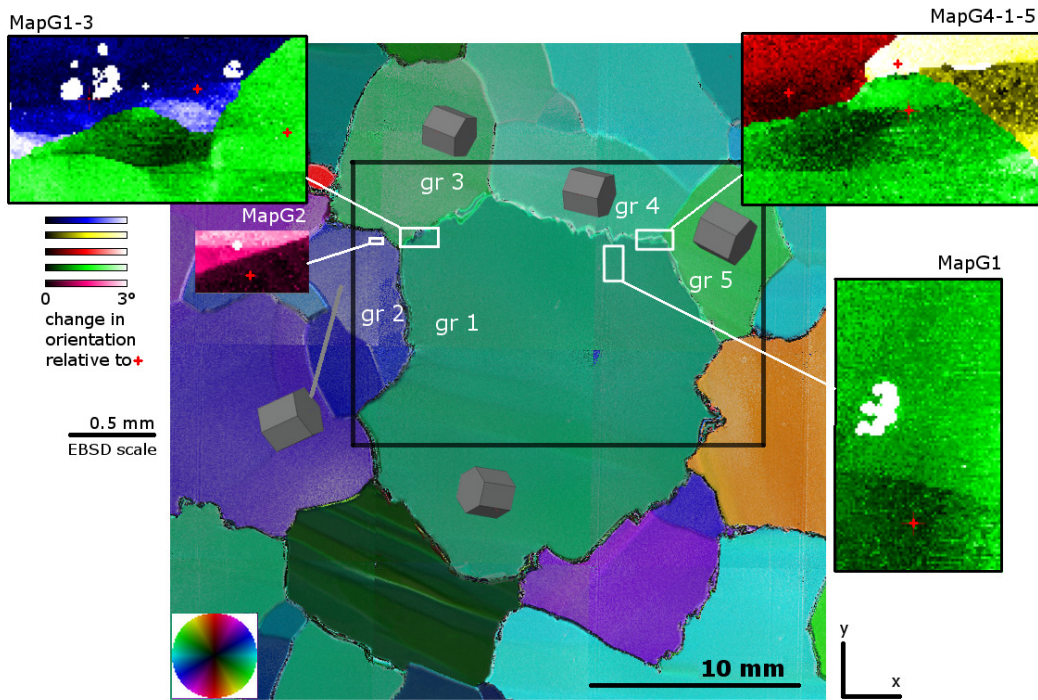


Figure 1: Microstructure of a selected area of the columnar ice sample (in the plane perpendicular to the columns) after compressive strain of 10% along y direction. The central microstructure is color coded according to the measured c-axis orientation as represented by the color wheel (inset). EBSD maps of selected areas (marked by white rectangles) are shown with color code for change in orientation according to color scheme provided on the left side of the central microstructure. Insets of 3D crystal orientations (grey hexagons) are provided by EBSD analyses. Grains are given numbers for ease of reference (e.g. gr 1). Note labeling of the selected areas for which EBSD maps were obtained corresponds to the grain numbers of the grains present in the respective map.

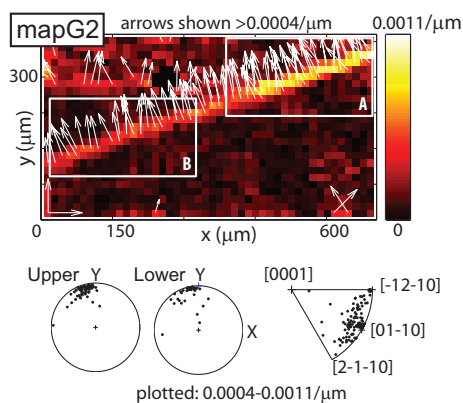


Figure 2: WBV magnitude (color range) for mapG2, WBV directions are shown as white arrows on map, above the threshold value for WBV magnitude of $0.0004/\mu\text{m}$, and on pole and inverse pole figures below. Areas analysed via integral WBV decomposition on crystallographic axes are marked as white boxes (A and B), corresponding data is given in Table 1. Note area A is in close vicinity to grain boundary.

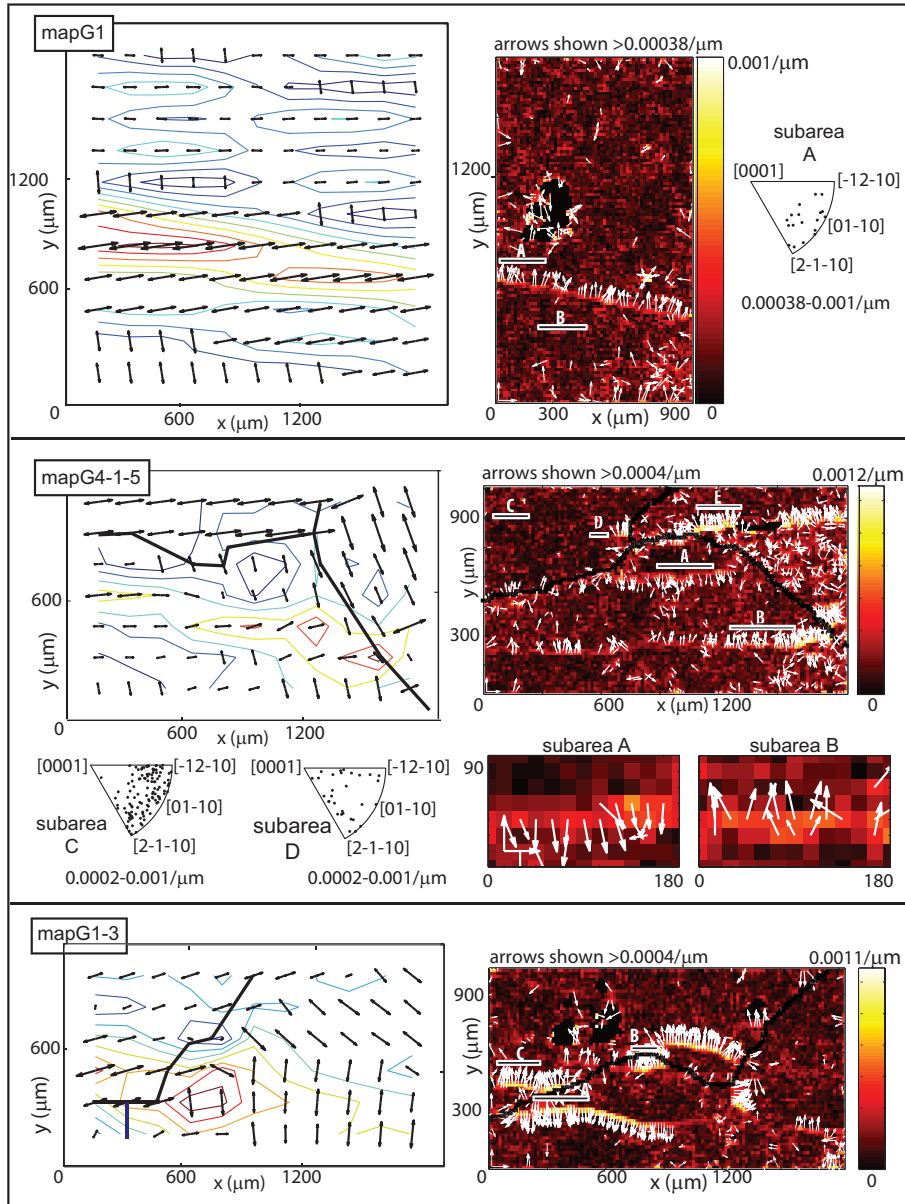


Figure 3: Comparison between stress field and dislocation field; deviatoric stress eigenvectors (left) zoomed in the areas selected for the WBV analyses (right maps). WBV analyses are shown with WBV magnitude (color range), WBV directions shown as white arrows on map (over a threshold value), and on inverse pole figures for selected areas (labeled A to D). Only upper limits are shown for these areas. Integral WBV of subareas are given in Table 1. Black lines represent grain boundaries. Due to limitation in the simulation configuration (see text), the correspondence between modeled and observed microstructures such as the position of grain boundaries is approximate.

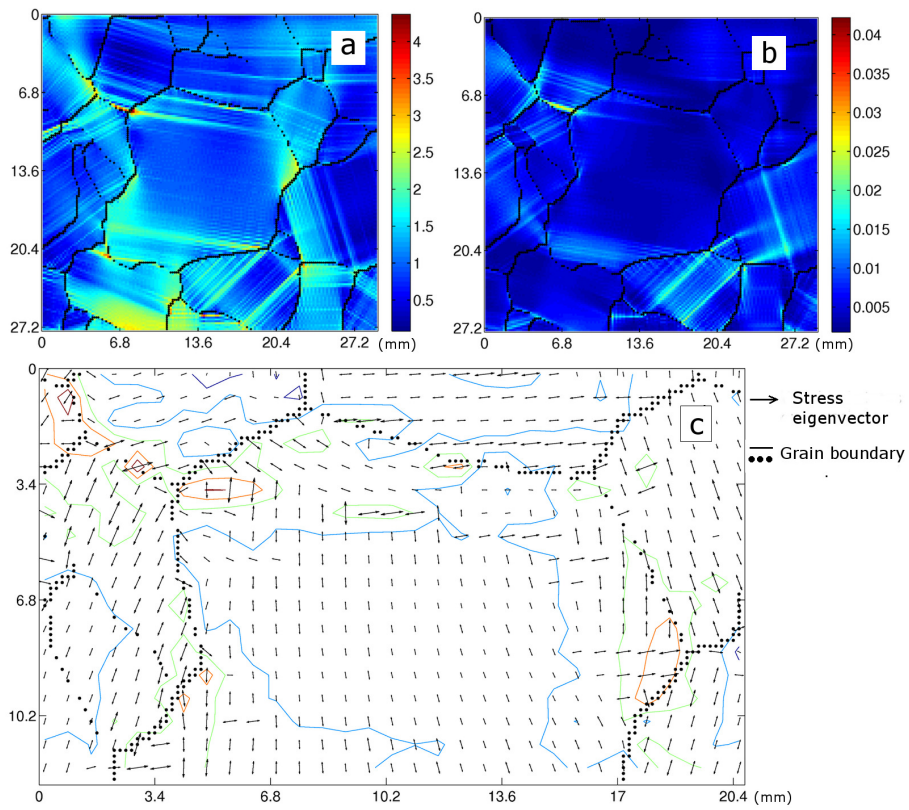


Figure 4: Maps of equivalent stress (in MPa) (a) and of equivalent strain (b) predicted by the full-field simulation using CraFT on the area of interest after 0.01 macroscopic strain under compression creep. c) provides a map of the deviatoric stress eigenvectors projected on the plane, superimposed on the equivalent stress contour plot (same scale as in a)). Grain boundary traces are superimposed for clarity but they are not physical entities in the code.

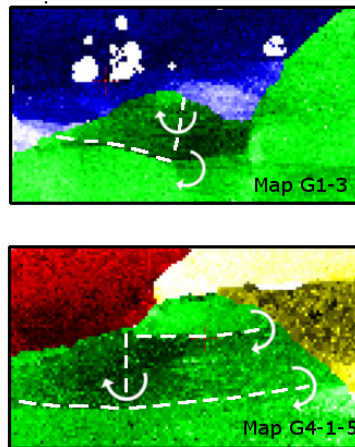


Figure 5: Planes of crystal bending (white stippled lines) for subgrain boundaries and associated rotation directions. The nearly horizontal subgrain boundaries are associated with abrupt misorientations, while the vertical ones correspond to more progressive misorientations. Both sub-structures were quantified in term of WBV, see Fig. 3.